Analyses and Optimization of Electrostatic Film Actuators Considering Electrical Breakdown

Yang Qu, Peisong Wang, Wenguang Wang, and Hongqiang Wang

Abstract—**Electrostatic film actuators are an emerging flexible actuation technique based on the electrostatic field. It is typically composed of two films (the stator and the slider), each of which integrates multiple phase interdigital electrodes. Since the structure and the electrical field distribution are complex, previous researches lack parameter analysis and optimization. Although recent study models and compares the output forces at the same voltage, the actuators of different parameters could survive at different critical voltages. With the concern on the electrical breakdown, this work is a preliminary attempt to analyze the maximum force and critical voltages for different specifications using the method of moments with line-charges. The computation results give qualitative clues about the optimization of various parameters. To achieve a higher maximum force, balancing the breakdown in the vertical gap and the horizontal gap is one of the primary concerns in the design. The theoretical maximum force for electrostatic film actuators can be achieved by different parameter sets: a large insulation layer and electrode space (high critical voltage) or a thin insulation layer and electrode space (low critical voltage). Based on this knowledge, we designed and fabricated an electrostatic film actuator with a force density of 126.5 N/m^2, 35% larger than the previous actuators at the same condition.**

Index Terms—**Electrostatic actuators, electrostatic film actuators, optimization, electrical breakdown.**

I. INTRODUCTION

ELECTROSTATIC actuators have become attractive for roboticists in the last decades since they are lightweight, compact, and flexible. Electrostatic film actuators (EFAs), as a flexible actuator, is an emerging electrostatic actuation technique [1], [2], as shown in Fig. 1(a). An EFA is typically composed of two identical electrode films, and each film is made by interdigital multiple-phase linear electrodes and insulation layers,
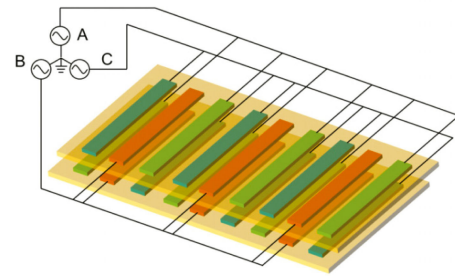
Fig. 1. The electrostatic film actuator. (a) The appearance of the electrostatic film actuator made in this work. (b) The principle and structure of the actuator. (c) Comparison of the output force of the EFAs made in this work and previous literature.

as shown in Fig. 1(b). When the electrodes are excited with multiple-phase voltage, the electrical potential introduces unlike charges on the electrodes. The shifting voltage on the electrodes generates a potential traveling wave and consequently moves the slider to slip on the stator. Since the primary material of EFAs is polymer insulators, the weight of the actuator is low. Besides,

ultrathin films make the actuator characterized by a low profile and remarkable compactness. EFAs can generate linear motion at a high precision since the movement is synchronous, and each step depends on the linear electrodes of tens micrometer thin. Due to these favorable features, EFAs are promising for extensive applications such as bioinspired robots, surgical robots, wearable robots, and inspection robots [3]–[8].

However, we still have little knowledge about selecting the optimal parameters since it becomes challenging considering the complex electrical field distribution and various interplaying parameters. Previously, researchers build finite element models to compare the influences of different parameters [9], [10]. Since the calculation costs enormous resources, the resultant data are usually sparse, insufficient for optimization. Recently we introduce the method of moments (MoM) into the study of the electrical field and the output force of EFA [11]. MoM is an integral method that solves Maxwell's Equation in integral form, contrasted to differential equations used in the finite element method. The MoM needs only to mesh electrodes and thus takes a shorter computation time, less computing resources, and comparable accuracy, compared with the finite element method.

In most previous studies, the actuators are compared and optimized by assuming different actuators work at the same magnitude of voltage [11]. This comparison makes sense in the theoretical analyses, but in practice, the actuators with thicker insulation and larger space between electrodes can resist a higher breakdown voltage and, maybe, generate a higher maximum force. Hence, to evaluate the ultimate capacities of various EFAs, we propose considering the corresponding critical breakdown voltages for each actuator as a key variable in the model instead of a constant that is typically assumed in the previous work [11]. For this purpose, we first build a mathematical model of the thrust force of EFA using MoM-Line. The MoM-Line model can generate more data with fewer computation resources and less duration. In the model, the breakdown strengths of the materials are listed as one of the key constraints of the output force. By analyzing the calculated results, this work discusses the qualitative relationship between the parameters and the maximum force and summarizes parameter selection strategies for the maximum output force of the actuators. Finally, we design and fabricate an EFA using a set of optimal parameters. This actuator can output a force (126.5 N/m^2) that is 30% stronger than that of the previous actuators at a similar working condition [4], [6], [12]–[14], as shown in Fig. 1(c).

The structure of this paper is as follows. The next section introduces the principle and modeling of MoM-Line. Section III analyzes the results and optimizes the parameters, and proposes the parameter optimization strategy. Section IV verifies the models by experiments and makes discussions.

II. MODELING OF EFAs BASED ON MoM-LINE

The modeling of EFA here is mainly based on the MoM-Line initially developed in our previous work [11]. The MoM-Line model assumes that each electrode in the actuator comprises a large number of arrayed line charges. Based on Coulomb's law, each charge generates an electrical field at a point in the actuator.

The net electrical field at this point is the superposition of all the electrical fields exerted by all the charges. Then we can have the electrical field distribution in the actuator and finally calculate the net driving force.

To facilitate the MoM-Line modeling, we first simplify the multiple layers of insulation into uniform insulation by ensuring the electrical field is the same. In the simplified model (with relative permittivity ε_1), the equivalent vertical distance between the electrodes can be derived by,

$$d = t_1 + t_2 + \frac{\varepsilon_1}{\varepsilon_2}g, \tag{1}$$

where t_1, t_2, and g are the insulation thickness of slider and stator films (relative permittivity ε_1) and the air gap (relative permittivity ε_2), respectively. Since the breakdown strength of the air (3.4 V/μm [15]) is less than 2% of that of the insulation materials (e.g., 220 V/μm for polyimide [16]), the breakdown of air is dominant in the analyses of the maximum force and voltage. The air layer is involved in the capacitors composed of overlapped electrodes (in the vertical direction of the model) and those containing coplanar electrodes (in the horizontal direction). In the equivalent model, we can conservatively assume that the insulation material's dielectric strength is the same as the air dielectric strength. Our experimental results verify this simplification, as discussed in Section IV.

We have the relationship between potential vector $U_{6N \times 1}$ and line charge vector $\Lambda_{6N \times 1}$,

$$U_{6N \times 1} = D_{6N \times 6N}\, \Lambda_{6N \times 1}. \tag{2}$$

The input voltage vector on the three-phase electrodes ($u_{6 \times 1}$ = [$\sin(\phi)$, $\sin(\phi - 2\pi/3)$, $\sin(\phi + 2\pi/3)$, $\sin(\phi + 2\pi/3)$, $\sin(\phi - 2\pi/3), \sin(\phi)$]) can be expressed by a potential vector,

$$U_{6N \times 1} = A_{6N \times 6}\, u_{6 \times 1}, \tag{3}$$

where $A_{6N \times 6}$ has the components as follows,

$$a_{ij} = \begin{cases} 1 & (j-1)N < i < jN \\ 0 & \text{others} \end{cases}. \tag{4}$$

On the other hand, according to Coulomb's law, the coefficient matrix $D_{6N \times 6N}$ can be achieved by,

$$D_{6N \times 6N} = \frac{1}{2\pi\varepsilon} \sum_{i=1}^{M} (\ln r_0 - \ln R_{6N \times 6N}), \tag{5}$$

where r_0 is the radius of a charged line, r_i is the distance from the aim point to the i-th charge line, λ is the charge density, ε is the permittivity of the insulation. $R_{6N \times 6N}$ is the relative distance matrix of different lines of charge, which can be represented by,

$$R_{6N \times 6N} = \sqrt{(X^T - X)^2 + (Y^T - Y)^2}, \tag{6}$$

where *X*, *Y* are the x-position and y-position matrixes of every line, which are expressed by,

$$X_{6N \times 6N} = B_1 \frac{a}{N} + B_2 p + x, \tag{7}$$

$$Y_{6N \times 6N} = Cd, \tag{8}$$

where the matrixes B_1, B_2 and C are dimensional coefficients. Thus, we can obtain the relationship between actuator structural parameters (a, s, p, d) and the coefficient matrix $D_{6N \times 6N}$.

The thrust force of the EFA is,

$$\mathbf{F} = \frac{1}{2\pi\varepsilon} \, g_{1 \times 3N}^T \frac{{}^{sl}\Lambda_{6N \times 1} \otimes {}^{st}\Lambda_{6N \times 1}}{{}^{lt}R_{3N \times 3N} *{}^{lt}R_{3N \times 3N}} \, g_{3N \times 1}$$

$$= F_{th} \, \mathbf{e_x} + F_{ad}\mathbf{e_y}, \tag{9}$$

where F_{th} is the ideal lateral thrust force, F_{ad} is the adhesive force between two films, $g_{3N \times 1}$ is a transformation vector, $\otimes$ is the operator of Kronecker product, and $*$ is the operator of Hadamard product. ${}^{sl}\Lambda_{6N \times 1}$ and ${}^{st}\Lambda_{6N \times 1}$ are the line charge density vectors in the slider film and the stator film, respectively. ${}^{lt}R_{3N \times 3N}$, ${}^{ll}R_{3N \times 3N}$, and ${}^{tt}R_{3N \times 3N}$ are the slider-stator relative position matrix, slider-slider relative position matrix, and stator-stator relative position matrix, respectively, inside of $R_{6N \times 6N}$,

$$R_{6N \times 6N} = \begin{bmatrix} {}^{ll}R_{3N \times 3N} & {}^{lt}R_{3N \times 3N} \\ {}^{lt}R_{3N \times 3N} & {}^{tt}R_{3N \times 3N} \end{bmatrix}, \tag{10}$$

among which ${}^{ll}R_{3N \times 3N}$ equals ${}^{tt}R_{3N \times 3N}$.

Considering the friction force generated by the normal adhesive force, the final actual thrust force $\hat{F}_{th}$ can be achieved by,

$$\hat{F}_{th} = F_{th} - \mu F_{ad}, \tag{11}$$

where μ is the friction coefficient.

III. PARAMETER ANALYSIS AND OPTIMIZATION UNDER THE CRITICAL VOLTAGE

Using the MoM-Line model mentioned above, here we evaluate the influence of parameters such as electrode width a, electrode space s, electrode pitch p, and the gap d to optimize the output force. To ensure the models' generalization, we normalize other parameters (e.g., the relative permittivity, the dielectric strength, and the voltage) in the following discussion. We can calculate the corresponding results for the specific materials by scaling the factors according to the equation,

$$F \propto \varepsilon V^2 \propto e_b^2, \tag{12}$$

where ε is the relative permittivity, V is the voltage, and e_b is the dielectric strength of the insulation material in the equivalent model.

A. Influence of the Horizontal Dimensional Parameters

Here we analyze the effects of the horizontal dimensional parameters, including a, s, and p, as shown in Fig. 2. They have a relationship of $a + s = p$.

The breakdown voltage can be approximately calculated by the product of the dielectric strength of the insulation material e_b and the distance between electrodes l,

$$V_l = e_b l. \tag{13}$$

In the following calculation, we normalize the breakdown voltage as 1 V for the reference distance of 100 μm ($e_b =$
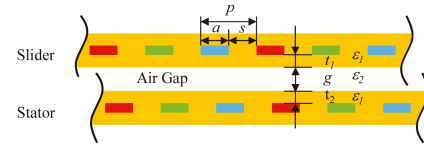

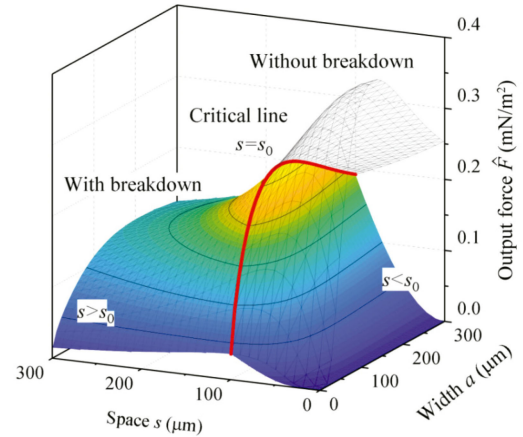Fig. 2. The schematic diagram of EFAs' parameters.

Fig. 3. The output force for various parameters. The colored surface and the grey mesh are the output force surfaces with and without consideration of breakdown, respectively. The intersection line between these two surfaces is marked by red. The area corresponds to the part covered by electrodes and gaps. The voltage for the case without concern on breakdown is 1 V. The force is calculated based on normalized relative permittivity, 1, and dielectric strength, 0.01 V/μm. Fig. 4–9 are also based on these assumptions.

0.01 V/μm) (to compare with the case without consideration of breakdown, in the model of which the electrodes are supplied with the voltage of 1 V) and assume the electrical field is uniform.

In an electrostatic actuator, the electrical breakdown might happen between the neighboring electrodes in the horizontal plane or between the two electrodes in the same vertical plane. The breakdown voltages are V_s ($= e_b s$) and V_d ($= e_b d$), respectively. The minimum one of them is the breakdown voltage of the whole actuator,

$$V = \begin{cases} V_d & V_d \le V_s \\ V_s & V_d > V_s \end{cases}. \tag{14}$$

In this section, we assume the vertical gap d is fixed, so V_d is constant. In the MoM-Line model, we apply the electrodes with a normalized voltage (V_0, 1 V) for the computation of force F. Accordingly, the output force $\hat{F}$ with the consideration of breakdown can be represented by,

$$\hat{F} = \frac{V^2}{V_0^2} \, F. \tag{15}$$

Based on this model, we can calculate the output force $\hat{F}$ at the breakdown voltage (the colored surface shown in Fig. 3) with variable a and s, assuming d is constant (100 μm), compared with the output force without the concern of breakdown (the grey mesh).

The maximum space for V_0 is $s_0 = V_0 / e_b$. If the space s is larger than s_0, the vertical direction is susceptible to breakdown,
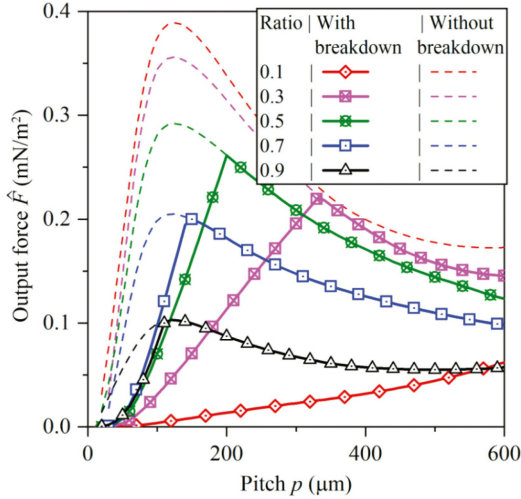
Fig. 4. Output force plots considering breakdown at various pitch, comparing with results without the concern of breakdown. The space ratio is $r = s/p$.
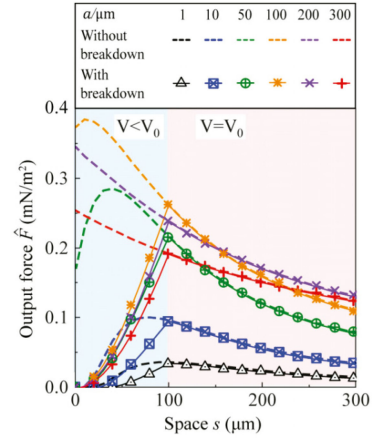

Fig. 5. Output force plots considering breakdown at various electrode spaces, comparing with the results without the concern of breakdown.
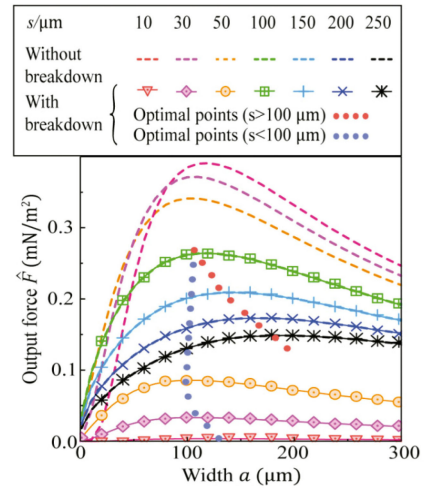

Fig. 6. Plots between output force and electrode width at various fixed spaces, comparing with the results without the concern of breakdown. The blue dotted lines fit the optimal points for s smaller than 100 μm, and the red for s larger than 100 μm.

the maximum voltage for the actuator is V_0, and the colored surface coincides with the grey mesh (the breakdown is more likely to happen in the vertical gap between electrodes) as shown in Fig. 3. In contrast, the space s that is smaller than s_0 makes the horizontal part weakest, the maximum voltage becomes V_s, and the colored surface is far below the grey mesh (the horizontal gap between electrodes is more prone to electrical breakdown).

If the electrical breakdown is not considered, the optimal pitch is the same for different space ratios ($r = s/p$) as discussed in our previous work [11]. Differently, when the limitation of an electrical breakdown is evaluated in the model, the optimal pitch changes depending on the space ratio (the solid lines in Fig. 4). This phenomenon perhaps results from the competition of the electrical breakdown of different places. When the horizontal space s between the electrodes is much smaller than the vertical gap d, the short circuit is apt to occur in the horizontal spaces. However, if the space is much larger than the vertical gap, the short circuit is most likely to happen in the vertical gap instead. When the space equals the vertical gap (100 μm), the force approaches the maximum value (see Fig. 5) since the breakdown capacities of these two insulation spaces are balanced at this moment.

As shown in Fig. 4, the output force becomes larger at first and then declines for increasing pitches. Perhaps it is because the electrodes disturb each other when they are too close in the horizontal plane, while they cannot generate equivalent force when the electrodes in different films are too far. If the breakdown is not considered, it seems the smallest space ratio is preferred. On another side, if the breakdown is the primary concern, the space ratio of 0.5 is better than the others (see the top points in Fig. 4) because a lower space ratio declines the breakdown voltage in the horizontal gap.

When the space ratio and the electrode space vary, the peak points always happen when the vertical gap is the same as the space, as shown in Fig. 6. Among them, the peak at the ratio of 0.5 makes the highest point. This is because the breakdown in the vertical gap and horizon gap should be balanced.

B. Influence of the Vertical Gap Between Electrodes

The actuator is subject to a breakdown not only in the horizontal space between electrodes but also in the vertical gap. Fig. 7 illustrates the output force $\hat{F}$ calculated by (15) at various vertical gap d. The gap must match up the space s and width a for the optimal output. For each d, there is a peak point on the data surface for the variables a and s. The peak ridge of every surface occurs at $d = s$, which is coincident with the tendency of the force for the constant vertical gap d as discussed in the last part.

Previously it is believed that a smaller vertical gap d always makes the force higher since the electrodes become closer. Therefore, a lot of efforts are made to circumvent the fabrication difficulties in reducing the horizontal gap and vertical gap [3], [17]. This is true if the voltage is the same, but for the case that the maximum output force is compared under the critical voltages, the results are quite different. Fig. 8 plots all the maximum force
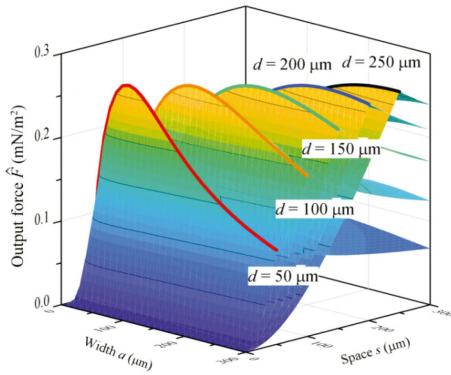
Fig. 7. Maximum output force at various equivalent gaps, where colored lines are the peak ridges of each surface.
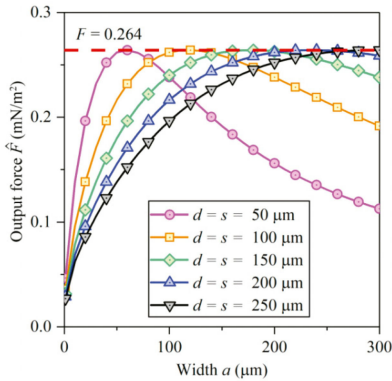

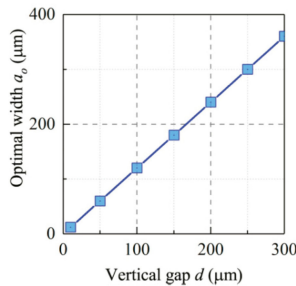Fig. 8. The optimal output force for different electrode widths.

Fig. 9. The optimal widths for film gaps while $d = s$.

of different parameters (the ridge curves ($d = s$) in Fig. 7). Two exciting phenomena become apparent: 1) the maximum output forces remain the same at different curves, 0.264 mN/m^2 (assuming the breakdown voltage is 1 V per 100 μm), and 2) the optimal a rises linearly with the equivalent gap (the optimal space is the same with the vertical gap) as shown in Fig. 9. The fitted function of a is found to be,

$$a_o = 1.2d. \tag{16}$$

The first phenomenon can be explained roughly by the simplified model of a parallel plate capacitor. The attractive stress

between the overlaid electrodes is,

$$f = 0.5\varepsilon \left(\frac{V}{d}\right)^2 = 0.5\varepsilon(e_b)^2. \tag{17}$$

This equation indicates that the maximum electrostatic force only depends on the material properties (e.g., permittivity and the dielectric strength), but has nothing to do with the dimensional parameters (e.g., the distance between electrodes). The second phenomenon can be explained by two aspects. The larger electrode width can generate a larger capacitance and capacitance variance (which directly decides the force magnitude [17]). Too large electrode, however, compresses the space since the whole area is constant and makes the actuator more susceptible to breakdown. The tradeoff of these two concerns induces the above optimal relationship shown in (16) for the parameters.

Therefore, to maximize its output force, we need firstly to choose the suitable equivalent film gap and the electrode space, making $d = s$, and then calculate the optimal electrode width a_0 using (16). The parameter selection strategy can be found in Fig. 10. Due to the above analyses, there is a large number of different optimal parameter sets (a, s, and d), but their maximum output force does not change theoretically. Among them, one option is to choose the comparatively small space and gap, where the output force per voltage is large, and the maximum voltage reduces significantly. Another alternative is to choose large space s and gap d, in which case the output force per voltage is small, but the maximum applicable voltage is high. These two solutions are both acceptable. The former solution brings many challenges to fabricate small space and electrode width, but it requires a lower voltage to achieve large enough output force, which is attractive for applications such as medical robots and consumer electronic devices. The latter solution has lower fabrication difficulty and cost, but it requires a higher voltage. These options give much flexibility to design for different applications.

C. Influence of Other Factors

The breakdown is indeed a complicated phenomenon involving various factors such as the material's properties, purity of the air, and even the humidity. In the equivalent model, the output force is proportional to the relative permittivity of the insulation layer, according to (12). The dielectric material with a higher relative permittivity can directly strengthen the output force. As shown in Fig. 11, for instance, if the relative permittivity of the insulation layer is 1 (the same as the air), the output force calculated from the equivalent model can be directly applicable. For the typical insulation, the output force increases linearly with the rising relative permittivity.

On the other hand, the insulation layer's dielectric strength influences the breakdown voltage and maximum force at a negligible level compared with the air since the air dielectric strength is approximately 2% of the insulation's. The dielectric strength of the air is more dominant for the breakdown of the actuator. Therefore, the environmental conditions are critical for the maximum output force. For instance, higher humidity, oxygen constituent, and pressure, which can raise the air dielectric strength [18]–[20], benefit a stronger output force of the actuator.
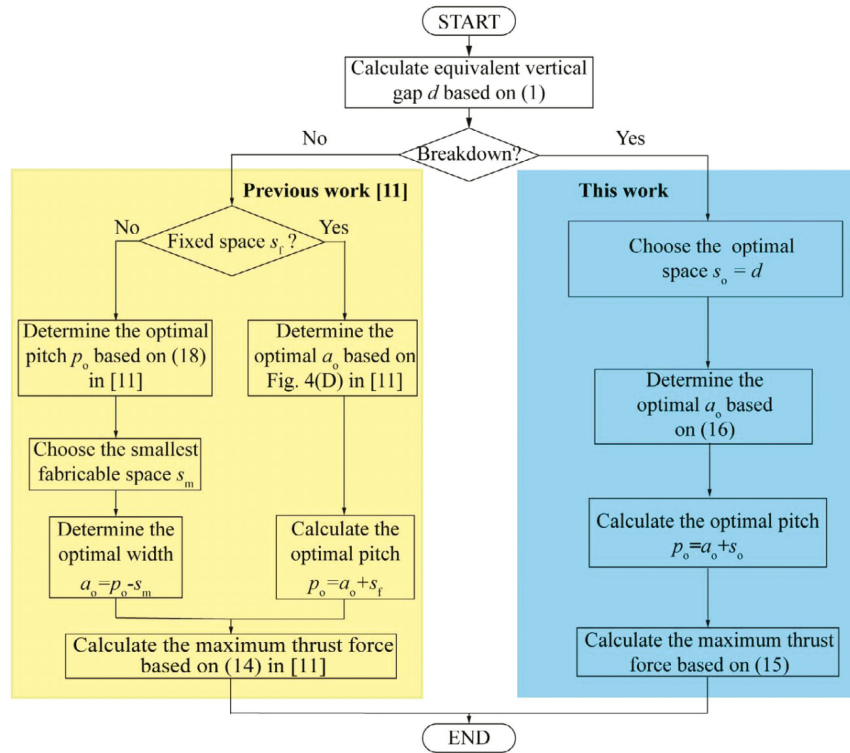
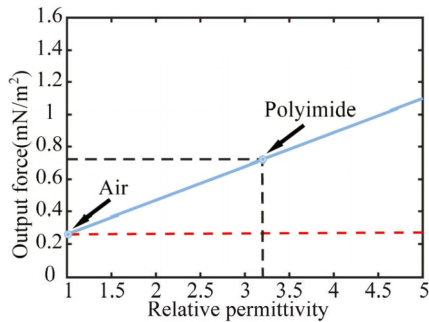Fig. 10.   Flow diagram of parameter optimization stategy for EFAs based on MoM-Line.

Fig. 11.   The relationship between relative permittivity and the output force.

IV. EXPERIMENTAL RESULTS AND DISCUSSION

A. Devise of an Electrostatic Film Actuator

Since the breakdown of the actuator is considered, based on the aforementioned optimization strategy, we need to select the space equal to the equivalent vertical gap. The insulation film can be made with the thickness of $t_1 = t_2 = 38$ μm according to our fabrication condition. The air gap thickness can be assumed as $g = 20{\sim}40$ μm empirically. The dielectric constant of air and insulation layer are 1 and 3.2 [21], respectively. According to (1), the equivalent gap is $140{\sim}204$ μm. Hence here, we design the space as 150 μm. Although the width of the electrode should be 1.2 times the space according to (16), it is selected to be the same as the space to facilitate the fabrication in this work. As shown in Fig. 7, little distinction from the optimal value on electrode

width does not reduce force significantly. Therefore, the pitch of the electrode is 300 μm.

The fabrication process is as follows. As shown in Fig. 12(a), we drill holes on a double laminated layer (25 μm polyimide base layer, 13 μm copper layer), including through-holes and location holes, using CNC. On the surfaces of through holes, carbon black is deposited by physical or chemical methods. By electrifying the carbon black electrodes, copper is plated on surfaces of the holes by the electroplating process, as shown in Fig. 12(b). When the electroplating is completed, photoresist layers are coated onto the two sides of the film. These photoresist layers stiffen when they are exposed to ultraviolet light. Fig. 12(c) shows the process of UV exposure with a mask. A developing solution (1% Na_2CO_3) reacts with unstiffened potions of the photoresist layers after UV exposure, as depicted in Fig. 12(d). Then etching solution ($CuCl_2$ and HCl) etches away the copper unprotected by the stiffened photoresist layers, as shown in Fig. 12(e). After peeling residual photoresist layers, the flexible circuit is covered by adhesive layers (13 μm) and polyimide layers (25 μm) using thermo-compression (2 MPa, 170 °C), as shown Fig. 12(f).

The final electrode films are shown in Fig. 1(a). Its thickness is 88 μm on average, and the weight of each film is 0.65 g. The length and width of the actuators are 105 mm and 43 mm, respectively, and the effective actuation area is 3195 mm^2 (90 mm $\times$ 35.5 mm).

B. Experiments and Discussion

Using the electrostatic film actuators fabricated based on the optimized parameters, we tested the output force by a load cell
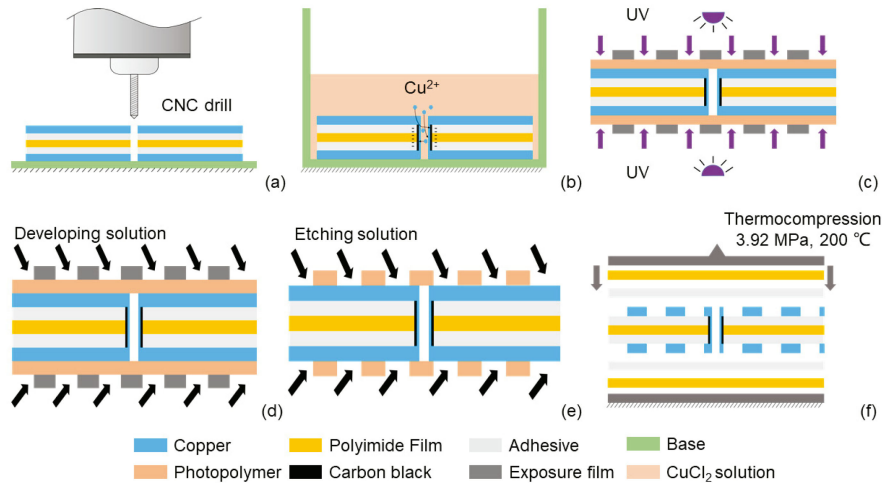
Fig. 12.   The fabrication process of an EFA. (a) Drill the holes. (b) Electroplating. (c) UV exposure with masks. (d) Remove the photoresist layer with developing solution. (e) Chemical etching of the conductive layer. (f) Cover the conductive layer with insulation layers by thermocompression.
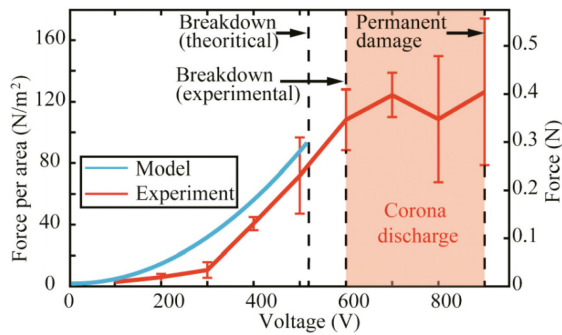

Fig. 13.   The output force of the EFA made in this work.

(LSB200, FUTEK). Its thrust force for a variety of voltage is shown in Fig. 13, compared with the estimation using the model introduced in this work. In the modeling, the dielectric constant is 3.2 [21]. Since the actual material is composed of multiple layers, including polyimide and air, conservatively, we select the dielectric strength of air (3.4 V/μm) [15] for calculation according to (12).

As shown in Fig. 13, the output force of the EFA increases with the voltage, as estimated in the model. The maximum force (91.6 N/m^2) in the model appears at 510 V. In the experiments, the actuator is safe until 600 V, and the voltage with higher magnitude causes a breakdown in the air and hiss noise (corona discharge). The corona discharge becomes more frequent and prominent when the voltage increases. When the voltage is 900 V, permanent damages occur, and the actuator can no longer operate. This result enlightens us to fill the air gap with a dielectric of higher electrical strength or to reduce the air bubbles in the electrode film using a more advanced fabrication process for a stronger output force in the future. The current EFA's output force is also much larger than the previous similar actuators shown in Fig. 1(c). The previous maximum magnitude of electrostatic film actuators is 93.7 N/m^2 [13], but the actuator's

output force in this work is 35% larger than this value due to the optimized parameters.

V. CONCLUSION

This paper builds a mathematical model to analyze the electrostatic film actuators' maximum output force with different parameters using MoM-Line. Unlike previous literature, this work considers the effects of the breakdown on the actuators of various parameters. The calculation results indicate two essential clues for optimal design. First, the horizontal space between electrodes should be equal to the equivalent vertical gap. Second, the maximum force for the larger pitch and thinner pitch can be of the same magnitude since the larger pitch can stand for a larger critical voltage. Based on these conclusions, this work devises an electrostatic film actuator with a 126.5 N/m^2 output force, 35% stronger than previous similar actuators.

This work considers the breakdown model of an actuator with a solid dielectric and a uniform electrical field, but the actual scenarios can differ. In the future, based on this model, we can further analyze the influences of more complex electrode shapes, composite materials, and electrode films on EFAs.

REFERENCES

[1] T. Higuchi, "Next generation actuators leading breakthroughs," *J. Mech. Sci. Technol.*, vol. 24, no. 1, pp. 13–18, 2010.
[2] W. S. N. Trimmer and K. J. Gabriel, "Design considerations for a practical electrostatic Micro-motor," *Sensors Actuators,* vol. 11, no. 2, pp. 189–206, 1987.
[3] H. Wang, A. Yamamoto, and T. Higuchi, "A crawler climbing robot integrating electroadhesion and electrostatic actuation," *Int. J. Adv. Robot. Syst.*, vol. 11, no. 12, pp. 191, 2014.
[4] H. Wang and A. Yamamoto, "Analyses and solutions for the buckling of thin and flexible electrostatic inchworm climbing robots," *IEEE Trans. Robot.*, vol. 33, no. 4, pp. 889–900, Aug. 2017.

[5] H. Wang and A. Yamamoto, "Peel force of electrostatic adhesion in Crawler-type electrostatic climbing robots," *J. Jpn. Soc. Appl. Electromag. Mechanics,* vol. 23, no. 3, pp. 498–503. 2015.

[6] H. Wang and A. Yamamoto, "A thin electroadhesive inchworm climbing robot driven by an electrostatic film actuator for inspection in a narrow gap," in *Proc. Int. Symp. Saf. Secur. Rescue Robot.*, 2013, pp. 1–6.

[7] Z. Zhang, N. Yamashita, M. Gondo, A. Yamamoto, and T. Higuchi, "Electrostatically actuated robotic fish: Design and control for high-mobility open-loop swimming," *IEEE Trans. Robot.*, vol. 24, no. 1, pp. 118–129, Feb. 2008.

[8] T. Hosobata, A. Yamamoto, and T. Higuchi, "Transparent synchronous electrostatic actuator for long-stroke planar motion," *IEEE/ASME Trans. Mechatronics*, vol. 20, no. 4, pp. 1765–1776, Aug. 2015.

[9] H. Wang, A. Yamamoto, and H. Toshiro, "The effect of parameters on the output forces of the integration of electroadhesion and electrostatic actuation considering breakdown voltage," in *Proc. JSPE Spring Conf.*, 2014, pp. 259–260.

[10] G. Zhang and A. Yamamoto, "Comparative analysis for sensorless displacement estimation of electrostatic film motors in different motor configurations," in *Proc. IEEE Int. Conf. Ind. Technol.*, 2019, pp. 163–168.

[11] W. Wang *et al.*, "Modeling and optimization of electrostatic film actuators based on the method of moments," in *Proc. Soft Robot.*, to be published, 2020.

[12] R. Yeh, S. Hollar, and K. S. J. Pister, "Single mask, large force, and large displacement electrostatic linear inchworm motors," *J. Microelectromech. Syst.*, vol. 11, no. 4, pp. 330–336, 2002.

[13] S. Tapuchi and D. Baimel, "Novel multilayer differential linear electrostatic motor," in *Proc. Int. Symp. Power Electron., Elect. Drives, Automat. Motion,* 2014, pp. 1368–1372.

[14] W. C. Tang, M. G. Lim, and R. T. Howe, "Electrostatic comb drive levitation and control method," *J. Microelectromech. Syst.*, vol. 1, no. 4, pp. 170–178, 1992.

[15] L. M. Apgar, "A study of the dielectric strength of air," M.S. dissertation, Dept. Elect. Eng., Univ. Illinois, Chicago, IL, 1913.

[16] S. Diaham, S. Zelmat, M.-L. Locatelli, S. Dinculescu, M. Decup, and T. Lebey, "Dielectric breakdown of polyimide films: Area, thickness and temperature dependence," *IEEE Trans. Dielectrics Elect. Insul.*, vol. 17, no. 1, pp. 18–27, Feb. 2010.

[17] A. Yamamoto, T. Niino, and T. Higuchi, "Modeling and identification of an electrostatic motor," *Precis. Eng.*, vol. 30, no. 1, pp. 104–113, 2006.

[18] P. N. Mikropoulos, C. A. Stassinopoulos, and B. C. Sarigiannidou, "Positive streamer propagation and breakdown in air: The influence of humidity," *IEEE Trans. Dielectrics Elect. Insul.,* vol. 15, no. 2, pp. 416–425, Apr. 2008.

[19] D. Wu, L. Arevalo, M. Lundmark, J. Karlsson, and M. Larsson, "A laboratory study on the dielectric strength of air gaps with lower oxygen constituent under switching impulse voltage," in *Proc. IEEE 11th Int. Conf. Properties Appl. Dielectric Mater.*, 2015, pp. 156–159.

[20] E. Husain and R. S. Nema, "Analysis of paschen curves for air, N2 and SF6 using the townsend breakdown equation," *IEEE Trans. Elect. Insul.*, vol. EI-17, no. 4, pp. 350–353, Aug. 1982.

[21] X. Li *et al.*., "Significant enhancement in dielectric constant of polyimide thin films by doping zirconia nanocrystals," *Mater. Lett.*, vol. 148, pp. 22–25, 2015.